metals

MDPI

Article

Analysis of Relaxation Processes in HNS Due to Interstitial-Substitutional Pairs

Alessandra Fava, Roberto Montanari *, Maria Richetta and Alessandra Varone

Department of Industrial Engineering, University of Rome "Tor Vergata", Via del Politecnico 1, 00133 Rome, Italy; alessandra.fava@uniroma2.it (A.F.); richetta@uniroma2.it (M.R.); alessandra.varone@uniroma2.it (A.V.)
* Correspondence: roberto.montanari@uniroma2.it; Tel.: +39-06-7259-7182

Received: 8 June 2017; Accepted: 29 June 2017; Published: 2 July 2017

Abstract: Mechanical Spectroscopy (MS) tests have been performed on a high nitrogen (0.8 wt %) austenitic steel (HNS) with resonance frequencies in the range of kHz. Two sets of samples have been examined: the first set in an as-prepared condition, the second one submitted to a heat treatment of 2 h at 800 °C, which induces a discontinuous precipitation of Cr_2N phase. In both sets, the damping spectrum shows a broad peak whose position and shape is changed by the precipitation of Cr_2N phase. The results are explained by considering interstitial-substitutional (i-s) interactions.

Keywords: HNS; Cr_2N; damping; dynamic modulus; interstitial-substitutional interactions

1. Introduction

In austenitic steels, nitrogen induces solid solution strengthening, increases corrosion resistance, and stabilizes the γ phase [1–5]. The difficulty of producing High Nitrogen Steels (HNS) is due to the thermodynamic limit of the solubility of nitrogen in a liquid or solid state [6,7]. Nitrogen solubility in austenite does not exceed 0.4 wt % [2,8], and in the temperature range between 700 °C and 1000 °C [9,10], the discontinuous precipitation of chromium nitrides occurs, according to the reaction:

$$\gamma \rightarrow \gamma^* + Cr_2N. \quad (1)$$

The excellent properties of HNS are partially compromised by nitride precipitation in thermal processes (welding, heat treatments, hot forming, etc.), therefore, in the last decade, a lot of work has been devoted to this topic (see e.g., [11–18]).

The mechanical properties of HNS strongly depend on the interstitial (carbon and nitrogen) content, even in dilute concentrations. The evolution of interstitial systems is governed by interactions induced by stress due to the volume misfit between the octahedral sites in austenite and the size of the interstitial atoms occupying them. Evidence of clustering and ordering of nitrogen under the effect of stress interactions in 316LN austenitic stainless steel was given by Shankar et al. [19] through High Resolution Electron Microscopy (HREM), however a quantitative description of atomic structures like interstitial systems is a hard task.

Mechanical Spectroscopy (MS), based on damping and dynamic modulus measurements, is a technique that provides information on atomic mechanisms that cannot be otherwise investigated. Gavriljuk and co-workers [20–24] employed MS to highlight different physical phenomena connected to interstitials in austenitic steels.

Banov et al. [25,26] measured a relaxation peak in the austenitic steel Fe-18Cr-4Mn-0.4N (wt %) with activation energy H = 1.47 eV, and attributed the peak to the re-orientation of atom pairs formed by one nitrogen atom and one substitutional atom. Gavriljuk et al. [20] found two peaks with activation energies H_1 = 1.41 eV and H_2 = 1.10 eV in the alloy Fe-18Cr-16Ni-10Mn-0.21N (wt %), which were explained by the same physical mechanism.

The aim of the present paper is to describe the anelastic effects arising from different interstitial systems present in a HNS in an as-prepared condition and after annealing for 2 h at 800 °C, which is a treatment inducing the discontinuous precipitation of chromium nitrides.

The microstructure has been investigated through X-ray diffraction (XRD), optical microscopy (OM), and scanning electron microscopy (SEM).

2. Material and Experimental

The examined material is a high nitrogen austenitic steel prepared by Pressurized Electroslag Remelting (PESR) with the following nominal chemical composition: 20 Cr, 2.5 Mo, 17 Mn, 0.2 C, 0.8 N, and Fe to balance (wt %). Two sets of samples have been examined: the first set in an as-prepared condition, the second one submitted to a heat treatment of 2 h at 800 °C.

Damping and dynamic modulus measurements have been carried out on bar-shaped samples (60 mm × 7 mm × 0.5 mm) using the method of frequency modulation; the Vibrating Reed Apparatus VRA 1604 (CANTIL Srl, Bologna, Italy) employed in the experiments was previously described in detail in [27–29].

The damping factor Q^{-1} was determined from the logarithmic decay δ of flexural vibrations:

$$Q^{-1} = \frac{\delta}{\pi} = \frac{1}{k\pi} \ln \frac{A_n}{A_{n+k}}, \quad (2)$$

where A_n and A_{n+k} are the amplitudes of n-th and $n + k$-th vibrations, respectively.

The dynamic modulus E was calculated from the resonance frequency f:

$$f = \frac{m^2 h}{2\pi\sqrt{12}L^2}\sqrt{\frac{E}{\rho}}, \quad (3)$$

where m is a constant depending on the specific sample geometry (for a reed m = 1.875), ρ is the material density, and L and h are the length and thickness of the sample, respectively. The resonance frequencies were in the range of kHz, and the strain amplitude was kept lower than 1×10^{-5}. In all of the experiments, the samples have been heated up to 800 °C with a heating rate of 1.7×10^{-2} °C·s^{-1}.

After mechanical polishing, the material has been etched in a water solution of 10% HCl, $K_2S_2O_5$ (10 g/L), and NH_4HF_2 (24 g/L), then examined by means of OM (Union Optical Co., Ltd., Tokyo, Japan) and SEM (Hitachi S-2460N, Tokyo, Japan).

The samples have been analyzed by XRD (Philips, Eindhoven, The Netherlands) using Co Kα radiation (λ = 0.1789 nm). XRD spectra were collected in step-scanning mode with 2Θ steps of 0.05°, and a counting time of 2 s per step in the angular range of 40°–95°. High precision peak profiles of the most intense reflections were recorded with 2Θ steps of 0.005° and a counting time of 20 s per step.

The precipitates were extracted from the matrix, examined by XRD, and identified by comparing the spectra with the files of the Joint Committee on Powder Diffraction Standards-International Centre for Diffraction Data (JCPDS-ICDD) database. The steel was dissolved through an electrochemical method: solution (20% methylic alcohol + 80% HCl), stainless steel cathode, and potential of 1.5 V. Filters with pores of 0.1 μm have been employed for the extraction of the residue from the liquid.

3. Results and Discussion

3.1. As-Prepared Steel

The steel in an as-prepared condition is fully austenitic (see XRD spectrum in Figure 1a).

Figure 1b shows the structure of the material. The image analysis has been performed on 20 micrographs (500 ×) through the software LUCIA (Version 4.51, Za Drahou, Praha, Czech Republic, 1991–2000): the grain size is ~50 μm (sdv = 4.6), and some twins (indicated by red arrows) are observed. The surface also exhibits small pores arising from the preparation route.

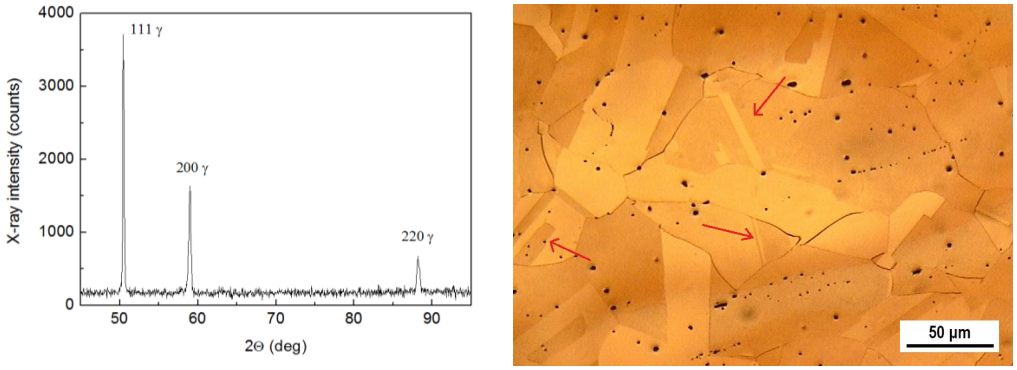

Figure 1. (**a**) XRD spectrum of the as-prepared material. (**b**) Microstructure of the steel.

Figure 2 displays the trends of Q^{-1} and E, normalized to E_0, vs. temperature; the value E_0 of an elastic modulus at room temperature is 196 GPa.

The Q^{-1} experimental data (full blue circles) are the superposition of an exponentially increasing background (black line) and a broad peak (open red circles). It is observed that the modulus (green squares) slope changes in correspondence of the Q^{-1} peak.

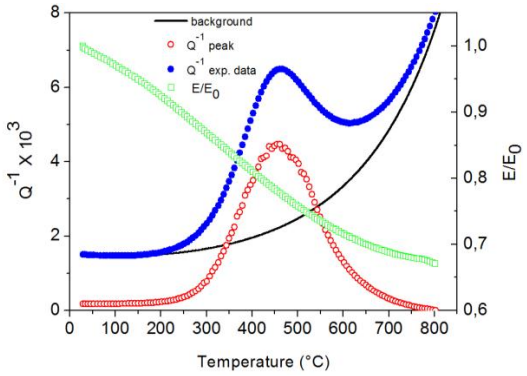

Figure 2. Q^{-1} and E, normalized to the room temperature value E_0, are reported vs. temperature. The Q^{-1} curve (full blue circles) is the superposition of a broad peak (open red circles) and an exponentially increasing background (black line). Resonance frequency f = 750 Hz.

Tests carried out with different resonance frequencies display the shift of Q^{-1} s peak position (see Figure 3) indicating that its origin is connected to relaxation processes, as confirmed by the slope change of the dynamic modulus E in correspondence of the peak.

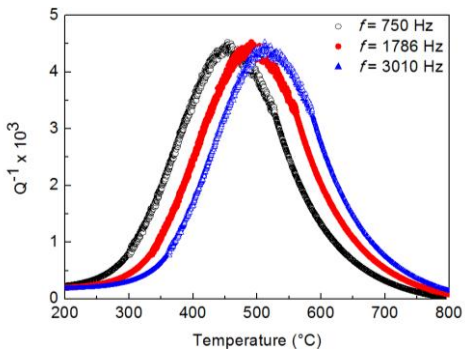

Figure 3. Q^{-1} peaks obtained in tests with three different resonance frequencies.

The temperature T_P of a relaxation peak depends on the resonance frequency f:

$$\omega\tau = 2\pi f \tau_0 e^{\frac{H}{RT_P}} = 1, \quad (4)$$

where H is the activation energy and R is the gas constant, while the relaxation time τ is given by:

$$\tau = \tau_0 e^{\frac{H}{RT_P}}, \quad (5)$$

where τ_0 is the pre-exponential factor that depends on the distribution of substitutional atoms in the nearest atomic shells around the pairs reorienting under the externally applied stress.

Tests with six different resonance frequencies (445 Hz, 750 Hz, 1033 Hz, 1786 Hz, 3010 Hz, and 5545 Hz) were carried out to determine H and τ_0. From the Arrhenius plot in Figure 4a, H = 1.76 eV and $\tau_0 = 2.23 \times 10^{-16}$ s have been obtained. However, the Q^{-1} peak displayed in Figure 2 is too broad and cannot be fitted by a single Debye peak, described by the relationship:

$$Q^{-1}(T) = \frac{\Delta}{2}\text{sech}\frac{H}{R}\left(\frac{1}{T} - \frac{1}{T_P}\right), \quad (6)$$

where $\Delta/2$ is the peak maximum. This means that the peak is not due to a single relaxation process, and H = 1.76 eV represents a pseudo activation energy.

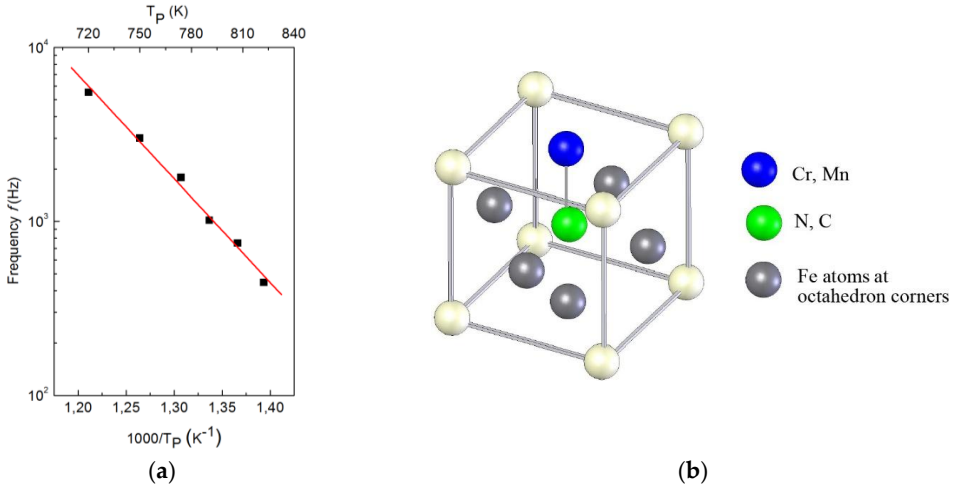

Figure 4. Arrhenius plot obtained from tests with six different resonance frequencies (**a**). Interstitial-substitutional (i-s) pairs in an fcc lattice of High Nitrogen Steel (HNS) (**b**).

The steel consists of a nitrogen supersaturated austenitic phase where carbon is also present, thus the origin of the peak has been ascribed to the re-orientation of interstitial-substitutional (i-s) pairs under the periodic externally applied stress [30]. Figure 4b displays a sketch of the i-s pairs in an fcc lattice of HNS steel.

The main substitutional elements are Cr and Mn, thus both of them could form pairs with the interstitial atoms (N and C). However, for resonance frequencies of the order of kHz used in the present experiments, the activation energy of C-Cr and N-Cr pairs [31] gives rise to peaks in a completely different range of temperatures. Therefore, only C-Mn and N-Mn pairs contribute to the energy dissipation giving rise to the observed peak.

On these grounds, a further attempt to fit the Q^{-1} peak was made by considering two Debye peaks due to the re-orientation of N-Mn and C-Mn pairs. For the re-orientation of N-Mn pairs, the values H = 1.76 eV [31] and $\tau_0 = 2.23 \times 10^{-16}$ s have been used. For the second process, namely the re-orientation of C-Mn pairs, the values H = 1.50 eV and $\tau_0 = 2.69 \times 10^{-15}$ s, determined by Kê

and Tsien [30] in the Fe-18.5 Mn alloy with a Mn content similar to that of the steel examined here, have been taken.

Since this fitting attempt also failed it has been assumed that each process is characterized by a single activation energy and a discrete distribution of relaxation times. The assumption reflects variations in the environment of the i-s pairs responsible for the relaxation, in particular the distribution of substitutional atoms in the nearest atomic shells around the i-s pairs reorienting under the externally applied stress.

For each relaxation process due to the reorientation of N-Mn and C-Mn pairs, instead of a single relaxation time τ, a series τ_n has been considered, which according to Equation (4) leads to n Debye peaks centered at different $(T_P)_n$. Therefore, the Q^{-1} peak was fitted as the sum of two contributions, Q^{-1} $(T)_{\text{N-Mn}}$ and Q^{-1} $(T)_{\text{C-Mn}}$, due to N-Mn and C-Mn pairs, respectively. Each contribution is the sum of n Debye peaks related to different relaxation times τ_n:

$$Q^{-1}(T) = Q^{-1}(T)_{\text{N-Mn}} + Q^{-1}(T)_{\text{C-Mn}} = \left\{\sum_n \left(\frac{\Delta}{2}\right)_n \text{sech}\frac{H}{R}\left[\frac{1}{T} - \frac{1}{(T_P)_n}\right]\right\}_{\text{N-Mn}} + \left\{\sum_n \left(\frac{\Delta}{2}\right)_n \text{sech}\frac{H}{R}\left[\frac{1}{T} - \frac{1}{(T_P)_n}\right]\right\}_{\text{C-Mn}}. \quad (7)$$

The central values τ_0 of each relaxation times' distribution are those used in the previous attempt of fitting, namely 2.23×10^{-16} s for N-Mn pairs and 2.69×10^{-15} s for C-Mn pairs. The other τ_n and the corresponding heights $(\Delta/2)_n$ of the Debye peaks have been treated as adjustable parameters to get the best fit displayed in Figure 5a. The height of each Debye peak is proportional to the number of relaxing units, i.e., the i-s pairs involved in that single process. The specific i-s pair fraction involved in processes with relaxation time τ_n is obtained by dividing the height $(\Delta/2)_n$ of the nth peak by $\Sigma_n(\Delta/2)_n$. The distributions of relaxation times τ_n and the pair fractions of the Debye peaks used to get the best fit in Figure 5a are shown in Figure 5b.

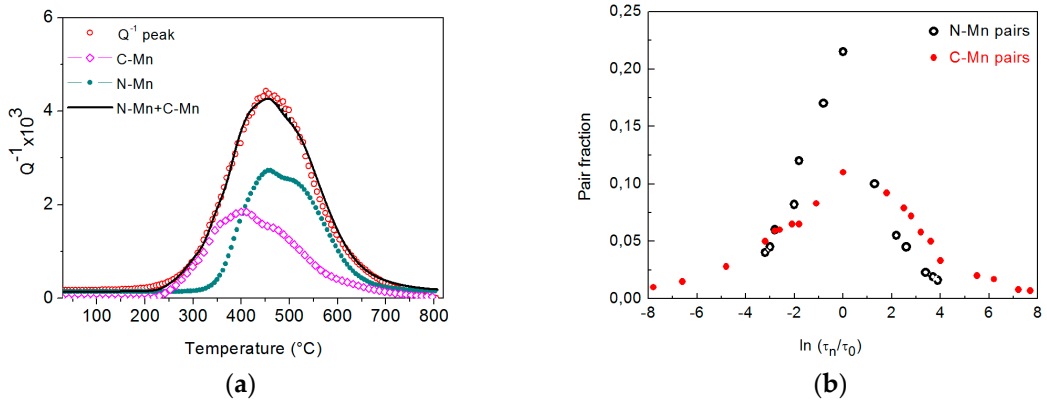

Figure 5. (**a**) Fitting of the broad Q^{-1} peak of as-prepared steel. (**b**) Distributions of relaxation times τ_n used to get the best fit displayed in (**a**).

The spread of relaxation times τ_n of C-Mn yields results quite larger than those of N-Mn. To give a tentative explanation of such difference, the specific characteristics of carbon and nitrogen have been considered. When dissolved in austenite, nitrogen and carbon atoms have nearly the same effective size, even if a little higher γ lattice dilatation due to nitrogen as compared to carbon was observed by some investigators (e.g., see [31]). More importantly, the electron density is increased in the vicinity of the interstitial sites occupied by nitrogen, whereas at the carbon sites their density is decreased [22]. As is well known, this involves important consequences on the mechanical behaviour and microstructure of austenitic steels:

- The increased density of free electrons due to nitrogen atmospheres near dislocations decreases the stress for activating dislocation sources and the line tension, thus nitrogen causes the early

start of plastic deformation and increases dislocation mobility. The effect of carbon on plasticity is the opposite.

- Nitrogen does not segregate substantially at grain boundaries, hence HNS exhibit good toughness and excellent resistance to intercrystalline corrosion, because the precipitation of chromium nitride at grain boundaries is very low when compared to that of chromium carbides.

It is reasonable that the remarkable increase of free electrons concentration near the nitrogen atoms located in the octahedral sites of the γ phase, and a more symmetrical distribution of electron density observed in the Fe-N austenite as compared to that in the Fe-C one [32,33], could affect the specific lattice positions occupied by the interstitials. In fact, the results displayed in Figure 5b are consistent with nitrogen atoms located at the centre of atomic shells with lower deviations of chemical composition than those of carbon.

3.2. Heat Treated Steel

As shown in Figure 6a,b, chromium nitrides, chromium carbides, and a transformed austenite γ* with a lower nitrogen content formed from the γ phase after the heat treatment at 800 °C. The typical discontinuous precipitation of the Cr-Mn-N system is described by Equation (1). Alternate lamellas of γ* and Cr_2N form and grow in the advancing interface between the transformed and untransformed zones, and the mean spacing between lamellas is ~190 nm (Figure 6b). In the transformed γ* austenite, precipitates of round shape are also observed. The precipitates, extracted from the matrix of heat treated steel, have been examined by XRD (Figure 7) and identified as: CrN (JCPDS-ICDD 11-65), Cr_2N (JCPDS-ICDD 35-803), and $Cr_{23}C_6$ (JCPDS-ICDD 35-783).

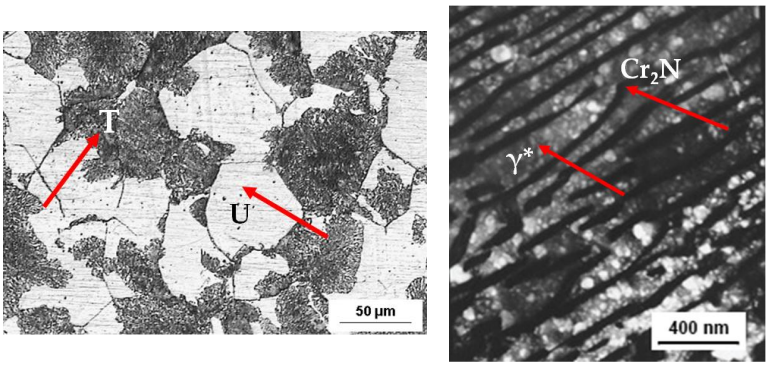

(**a**) (**b**)

Figure 6. Cellular precipitation after the heat treatment (**a**). Arrows indicate transformed (T) and untransformed (U) zones. SEM micrograph showing details of the lamellar structure made of γ* and Cr_2N (**b**).

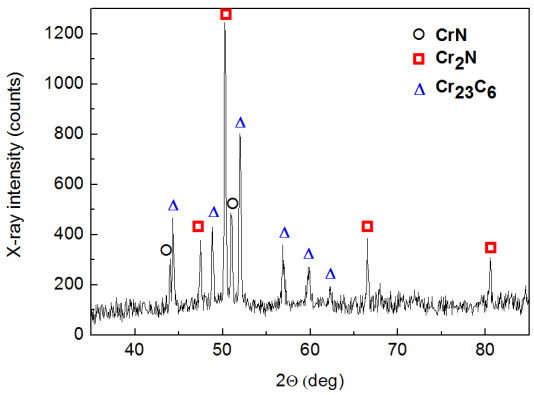

Figure 7. XRD spectrum of the precipitates extracted from the steel heat treated 2 h at 800 °C.

From an image analysis of the 30 OM micrographs taken at the same magnification (400×), the fraction of transformed material was estimated to be ~15%. The microstructure is characterized by two austenitic phases (γ and γ*) plus carbides and nitrides.

Figure 8 shows the precision peak profile of the (111) austenite reflection: the contributions of γ and γ* are clearly distinguished, because the γ* reflection is shifted to a higher angle. The lattice parameter of the secondary γ* austenite is smaller (0.3615 nm) than that of the supersaturated austenite γ (0.3636 nm), thus its nitrogen content is smaller.

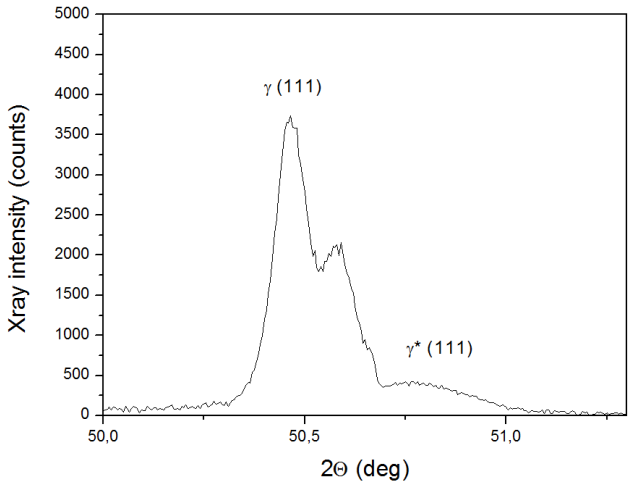

Figure 8. Contributions of γ and γ* to the precision (111) peak profile.

Figure 9 shows the trends of Q^{-1} and E/E_0 vs. temperature.

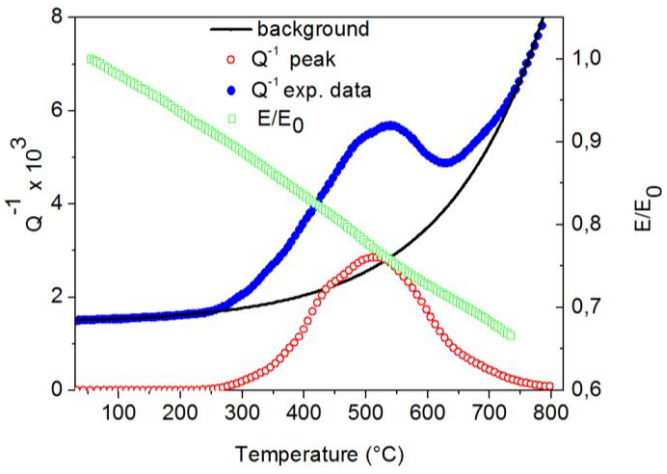

Figure 9. Q^{-1} and E/E_0 vs. temperature of the steel heat treated for 2 h at 800 °C. Resonance frequency f = 750 Hz.

Also in this case, the Q^{-1} curve is the superposition of a broad peak and an increasing background. The intensity of the background remains substantially unchanged while the peak temperature is about 80 °C higher than that of the untreated material. Background strongly depends on grain size and dislocation density, thus, since the heat treatment substantially does not change these factors [14], the background level is stable.

From tests with different frequencies, a pseudo activation energy of 1.92 eV was determined.

The peak shift to a higher temperature with respect to the as-received steel depends on the presence of the transformed austenite, therefore the re-orientation of N-Mn pairs in the γ* phase have

also been considered. The same procedure used to get the fitting shown in Figure 5 has been employed. The heat treatment induces a strong precipitation of $Cr_{23}C_6$ carbides (Figure 7), and as a consequence the carbon atoms free of contributing to relaxation processes decrease. We were able to fit the curve without considering the C-Mn pair in the γ* contribution. The results are displayed in Figure 10.

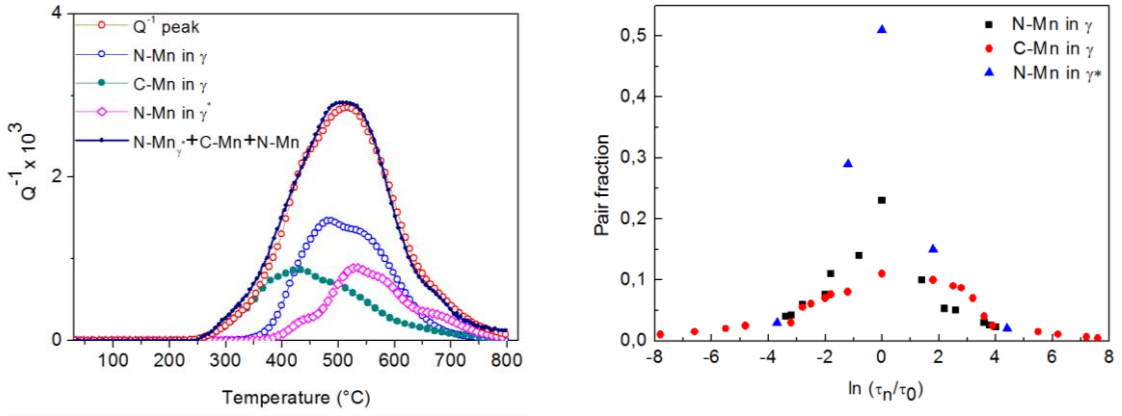

(**a**) (**b**)

Figure 10. (**a**) Fitting of the Q^{-1} peak of the heat treated steel. (**b**) Distributions of relaxation times τ_n used to get the best fit displayed in (**a**).

The area under the C-Mn and N-Mn pair contributions is proportional to the number of specific relaxation processes, namely the number of i-s pairs. Table 1 reports the area values of the i-s contributions, normalized to that of the Q^{-1} peak of the as-prepared material.

Table 1. Areas under specific i-s pair contributions, normalized to that of the Q^{-1} peak of the as-prepared material.

Material	N-Mn in γ Phase	C-Mn in γ Phase	N-Mn in γ* Phase	Total Area
As-prepared	0.5870	0.4130	-	1.000
Heat treated 2 h/800 °C	0.2724	0.1941	0.1571	0.6236

After heat treatment, the area of the C-Mn pairs' contribution decreases to about half of the original value. This is due to the formation of carbides that capture carbon, thus it is no longer available for relaxation processes. The N-Mn pairs are present in both austenitic phases (γ and γ*), but also in this case, the total contribution is quite lower than that in the as-prepared material owing to the formation of Cr nitrides.

As expected, the spread of relaxation times τ_n of C-Mn pairs is always larger than those of N-Mn pairs in both the γ and γ* phases. The distribution of τ_n for N-Mn pairs is quite similar to that of as-prepared steel, while the distribution in γ* is strongly peaked around τ_0. The result seems to indicate that the spread of τ_n depends on the state of the supersaturation of nitrogen, and decreases as nitrogen content approaches the value of thermodynamic solubility.

The origin of anelastic phenomena observed in present experiments is the re-orientation of i-s pairs, namely the same physical phenomenon giving rise to the Q^{-1} peaks found by Gavriljuk et al. [20] and Banov et al. [25,26] in similar steels with high nitrogen content. This work evidenced that the Q^{-1} peak is not a Debye peak due to a single relaxation process, but in fact it is the superposition of specific contributions from different types of i-s pairs. Moreover, each contribution consists of many relaxation peaks with a common activation energy and different relaxation times. The analysis we have carried out seems to be a useful tool to describe the states of not homogeneous chemical distribution on an atomic scale that can change following phase transformations occurring during heat treatments.

4. Conclusions

The Q^{-1} curves of HNS are the superposition of an exponential background and a broad peak.

The microstructure of steel consists of a nitrogen supersaturated γ phase, and the Q^{-1} peak is the sum of two contributions due to the re-orientation of N-Mn and C-Mn pairs. Each contribution has been analysed as the sum of a series of Debye peaks with the same activation energy but different relaxation times, reflecting variations in the distribution of substitutional atoms in the nearest atomic shells around the pairs reorienting under the externally applied stress.

After the heat treatment of 2 h at 800 °C, which leads to the partial transformation of the material, two austenitic phases γ and γ* are present. γ* is the transformed austenite with lower nitrogen content, therefore there is a further contribution to the Q^{-1} spectra due to the re-orientation of N-Mn pairs in the γ* phase.

Author Contributions: Roberto Montanari devised the experiments, Alessandra Varone and Alessandra Fava performed the Mechanical Spectroscopy and XRD experiments; Maria Richetta performed SEM and optical microscopy observations; all of the authors discussed the results and contributed to writing the paper.

Conflicts of Interest: The authors declare no conflict of interest.

References

1. Gavriljuk, V.G.; Berns, H. *High Nitrogen Steels Structure, Properties, Manufacture, Applications*; Springer Verlag: Berlin, Germany, 1999.
2. Simmons, J.W. An overview: High-nitrogen alloying of stainless steels. *Mater. Sci. Eng. A* **1996**, *207*, 159–169. [CrossRef]
3. Berns, H. Manufacture and application of high nitrogen steels. *ISIJ Int.* **1996**, *36*, 909–914. [CrossRef]
4. Di Schino, A.; Kenny, J.M. Effect of grain size on the corrosion resistance of a high nitrogen low nickel austenitic stainless steel. *J. Mater. Sci. Lett.* **2002**, *21*, 1969–1971. [CrossRef]
5. Ha, H.Y.; Kwon, H.S. Effects of Cr_2N on the pitting corrosion of high nitrogen stainless steels. *Elettrochim. Acta* **2007**, *52*, 2175–2180. [CrossRef]
6. Feichtinger, H.K.; Stein, G. Melting of high nitrogen steel. *Mater. Sci. Forum* **1999**, *318–320*, 261–270. [CrossRef]
7. Stein, G.; Menzel, J. Nitrogen alloyed steels—A new generation of materials with extraordinary properties. *Int. J. Mater. Prod. Technol.* **1995**, *10*, 290–302.
8. Hanninen, H.; Romu, J.; Ilola, R.; Tervo, J.; Laitinen, A. Effects of processing and manufacturing of high nitrogen-containing stainless steels on their mechanical, corrosion and wear properties. *J. Mater. Process. Technol.* **2001**, *117*, 424–430. [CrossRef]
9. Shi, F.; Wang, L.J.; Cui, W.F.; Liu, C.M. Precipitation behavior of M_2N in a high-nitrogen austenitic stainless steel during isothermal aging. *Acta Metall. Sin.* **2007**, *20*, 95–101. [CrossRef]
10. Dai, Q.X.; Yuan, Z.Z.; Luo, X.M.; Cheng, X.N. Numerical simulation of Cr_2N age-precipitation in high nitrogen stainless steels. *Mater. Sci. Eng. A* **2004**, *385*, 445–448. [CrossRef]
11. Knutsen, R.D.; Lang, C.I.; Basson, J.A. Discontinuous cellular precipitation in a Cr-Mn-N steel with niobium and vanadium additions. *Acta Mater.* **2004**, *52*, 2407–2417. [CrossRef]
12. Feng, S.; Wang, L.J.; Cui, W.F.; Liu, C.M. Precipitation kinetics of Cr_2N in high nitrogen austenitic stainless steel. *J. Iron Steel Res. Int.* **2008**, *15*, 72–77.
13. Yuan, Z.Z.; Dai, Q.X.; Cheng, X.N.; Chen, K.M. Microstructural thermostability of high nitrogen austenitic stainless steel. *Mater. Charact.* **2007**, *58*, 87–91. [CrossRef]
14. Mezzi, A.; Kaciulis, S.; Montanari, R.; Rovatti, L.; Ucciardello, N.; Carosi, A. Discontinuous precipitation in a high nitrogen austenitic steel. *Mater. Sci. Forum* **2010**, *638–642*, 3597–3602.
15. Carosi, A.; Gregoratti, L.; Kaciulis, S.; Mezzi, A.; Montanari, R.; Rovatti, L.; Ucciardello, N. Heating modification of an austenitic steel with high nitrogen content. *Surf. Interface Anal.* **2010**, *42*, 726–729. [CrossRef]
16. Shi, F.; Qi, Y.; Liu, C. Effects of Mo on the precipitation behaviors in high-nitrogen austenitic stainless steels. *J. Mater. Sci. Technol.* **2011**, *27*, 1125–1130. [CrossRef]

17. Li, J.Y.; Liu, H.N.; Huang, P.W. Effects of pre-precipitation of Cr_2N on microstructures and properties of high nitrogen stainless steel. *J. Cent. South Univ.* **2012**, *19*, 1189–1195. [CrossRef]
18. Kartik, B.; Veerababu, R.; Sundararaman, M.; Satyanarayana, D.V.V. Effect of high temperature ageing on microstructure and mechanical properties of a nickel-free high nitrogen austenitic stainless steel. *Mater. Sci. Eng. A* **2015**, *642*, 288–296. [CrossRef]
19. Shankar, P.; Sundararaman, D.; Ranganathan, S. Clustering and ordering of nitrogen in nuclear grade 316LN austenitic stainless steel. *J. Nucl. Mater.* **1998**, *254*, 1–8. [CrossRef]
20. Gavriljuk, V.G.; Foct, J.; Bugaychuk, S.N.; Sozinov, A.L. Relaxation phenomena in nitrogen austenitic steels. *Scr. Mater.* **1997**, *37*, 1889–1894. [CrossRef]
21. Gavriljuk, V.G.; Yakovenko, P.G.; Ullakko, K. Influence of nitrogen on vibration damping and mechanical properties of Fe-Mn alloys. *Scr. Mater.* **1998**, *38*, 931–935. [CrossRef]
22. Gavriljuk, V.G.; Shivanyuk, V.N.; Shanina, B.D. Change in the electron structure caused by C, N and H atoms in iron and its effect on their interaction with dislocations. *Acta Mater.* **2005**, *53*, 5017–5024. [CrossRef]
23. Gavriljuk, V.G. Austenite and martensite in nitrogen-, carbon- and hydrogen-containing iron alloys: Similarities and differences. *Mater. Sci. Eng. A* **2006**, *438–440*, 75–79. [CrossRef]
24. Teus, S.M.; Shyvanyuk, V.N.; Gavriljuk, V.G. On a mechanism of Snoek-like relaxation caused by C, N and H in fcc iron-based alloys. *Acta Mater.* **2006**, *54*, 3773–3778. [CrossRef]
25. Banov, R.M.; Parshorov, I.M.; Kamenova, C.Z. A model of relaxation in nitrogen austenitie steels. *Izvestia AN SSSR* **1978**, *3*, 178–182. (In Russian)
26. Banov, R.M.; Parshorov, I.M.; Kamenova, C.Z. Relaxation phenomena in austenitie steels alloyed by nitrogen. *Izvestia AN SSSR* **1978**, *1*, 126–129.
27. Amadori, S.; Campari, E.G.; Fiorini, A.L.; Montanari, R.; Pasquini, L.; Savini, L.; Bonetti, E. Automated resonant vibrating-reed analyzer apparatus for a non-destructive characterization of materials for industrial applications. *Mater. Sci. Eng. A* **2006**, *442*, 543–546. [CrossRef]
28. Balijepalli, S.K.; Colantoni, I.; Donnini, R.; Kaciulis, S.; Lucci, M.; Montanari, R.; Ucciardello, N.; Varone, A. Elastic modulus of S phase in kolsterized 316L stainless steel. *Metallurgia Italiana* **2013**, *105*, 42–47.
29. Balijepalli, S.K.; Donnini, R.; Kaciulis, S.; Montanari, R.; Varone, A. Young's modulus profile in kolsterized AISI 316L steel. *Mater. Sci. Forum.* **2013**, *762*, 183–188. [CrossRef]
30. Nowick, A.S.; Berry, B.S. *Anelastic Relaxation in Crystalline Materials*; Academic Press: Cambridge, MA, USA, 1972; p. 454.
31. Blanter, M.S.; Golovin, I.S.; Neuhauser, H.; Sinning, H.-R. *Internal Friction in Metallic Materials*; Springer Verlag: Berlin, Germany, 2007.
32. Cheng, L.; Bottger, A.; de Keijser, T.H.; Mitttemeijer, E.J. Lattice parameters of iron-carbon and iron-nitrogen martensites and austenites. *Scr. Metall. Mater.* **1990**, *24*, 509–514. [CrossRef]
33. De Cristofaro, N.; Kaplow, R. Interstitial atom configurations in stable and metastable Fe-N and Fe-C solid solutions. *Metall. Trans. A* **1977**, *8*, 35–44. [CrossRef]